APCC
APEC CLIMATE CENTER

TECHNICAL REPORT

APCC
APEC CLIMATE CENTER

PREFACE

It is our pleasure to present to you the APEC Climate Center (APCC)'s Technical Report 2012, which reports the core outcomes of our research activities from the past year.

Since 2005, APCC, as a hub of climate information in the Asia-Pacific region, has strived to share our analysis and prediction of abnormal climate and to apply this information to regional development. The Center has established the most extensive Multi-Model Ensemble (MME) system for seasonal prediction in the world through its international science network and has provided value-added products to various stakeholders. Recently, APCC has expanded its mandate to include enhancing the capacity of APEC member economies to respond effectively to climate change and variability through better application of climate information.

In 2012, APCC continued to make an effort to improve the quality and quantity of our short-term climate forecasts and our online climate information systems, as information dissemination tools. Additionally, APCC began its endeavor to produce more applicable climate information through interdisciplinary research among various sectors, such as agriculture and hydrology. The following technical report provides more information about our research outcomes from 2012.

In 2013, following APCC's goal to enhance socioeconomic well-being through better utilization of climate information, APCC will continue to improve the quality and accuracy of its climate information, recognizing that the utility of this information is only as good as its quality. We would like to make the best use of our research outcomes in various scientific and application areas. We welcome any feedback on this report or on our services.

My best and warmest regards to all of you.

Dr. Chin-Seung Chung
Director/APEC Climate Center

CONTENTS

Evaluation of a Distributed Hydrologic Model with TRMM 3B42 and its Application in the Nakdong-River Basin, South Korea

Mr. Jongpil, Kim

APCC
TECHNICAL REPORT 2012-02

Evaluation of a Distributed Hydrologic Model with TRMM 3B42 and its Application in the Nakdong-River Basin, South Korea

Mr. Jongpil, Kim

ABSTRACT

The performance of the Coupled Routing and Excess Storage (CREST) distributed hydrologic model, developed by the University of Oklahoma in collaboration with the NASA for the SEVIR project, was evaluated in the Nakdong-River Basin, South Korea. From the Nakdong-River Basin, five mid-scale basins with multipurpose dams were selected for study. Tropical Rainfall Measuring Mission (TRMM) Multi-satellite Precipitation Analysis (TMPA) products were applied to the target basins and the mean areal precipitation (MAP-R) was computed and compared to that of ground based raingauge network (MAP-G). Results showed that MAP-R overestimated precipitation from 2002 to 2010 in all the target basins. A comparison between MAP-R and MAP-G generated poor statistics, including those of the correlation coefficient and root mean squared error.
This study demonstrates that the CREST model combined with MAP-G performs well in all the target basins, but the MAP-R contains errors that affect hydrological simulation. These errors originate from the limitation of remote sensor using microwaves and could be reduced by employing a statistical adjustment. Satellite-based precipitation datasets are expected to provide more accurate and reliable hydrologic modeling.

1. INTRODUCTION

Knowledge of the spatial and temporal distribution of water over the landscape is important for water management strategies and for implementing coping strategies in relation to water-related natural disasters (Wang *et al.*, 2011). Hydrologic models, which work in accordance with consideration of the spatial heterogeneity of hydrological state variables, can provide information to assist with these strategies. Two major types of hydrologic models exist; lumped models and distributed models. The parameters of lumped models are relatively conceptual and empirical in comparison with the distributed models and in an initial simulation they show a low accuracy. In order to improve this they can be adjusted using an optimization scheme such as a trial and error method or neural networks (Park, 2010). However, the physically-based distributed models show a somewhat higher performance and need only slight adjustment for the model parameters (Hong *et al.*, 2006).

With the recent growth of microwave remote sensing and Geographical

Information System (GIS) technology, physically-based distributed hydrologic models are increasingly developed for scientific and technical purposes, such as water resources management, climate change impact assessment, prediction of streamflow in an ungauged catchments, and the investigation of spatial distribution of hydrological variables (Moretti and Montanari, 2007). However, most research using hydrologic modeling is conducted on the watershed scale. To gain a better understanding of the local hydrological processes that occurr in a catchment, it is preferable to use highly dense information for hydrological simulation. The advantage of this approach is that the accuracy of flood prediction can be improved and the spatio-temporal distribution of water can be closely examined. However, the application may be limited to the short-term forecast of runoff within the local region due to the deficit of meteorological measurements and a lack of high resolution surface information; an inherited trait of rainfall-runoff modeling techniques.

Because of these limitations in watershed modeling, a macroscale hydrological analysis with satellite remote sensing data is required for the examination of water balance, climate change, land cover change, integrated water management and change impact on water resources on a global- and continental-scale.

Many hydrologic models have been developed to investigate the spatial and temporal distribution of water over a broad landscape. Liang *et al.* (1994, 1996) developed a semi-distributed macroscale hydrologic model, the Variable Infiltration Capacity (VIC) model, suitable for incorporation in General Circulation Models (GCMs). The notable features of the model include subgrid variability in surface vegetation classes and soil moisture storage capacity, calculation of baseflow, and the inclusion of topography. Hagemann and Dümenil (1998, 2001) developed a hydrologic model for the simulation of lateral waterflow on a global scale, which describes the translation and retention of lateral discharge as a function of the spatially distributed land surface characteristics. Alcamo *et al.* (2003) developed a global water assessment model, "WaterGAP 2", which consists of a global water use model and a global hydrologic model. Each component was tested in several rivers and the outputs were analyzed. Wang *et al.* (2011) developed a distributed hydrologic model, the Coupled Routing

and Excess Storage (CREST) model, which included the generation of rainfall-runoff, evapotranspiration, sub-grid cell routing, downstream routing and feedbacks between the routing and rainfall-runoff modules.

Simultaneously, many studies on link between satellite precipitation estimates and a hydrologic model or a water balance model have been conducted. Qin *et al.* (2008) retrieved evapotranspiration from the MODerate resolution Imaging Spectroradiometer (MODIS) products using the Surface Energy Balance System (SEBS) algorithm. And they examined the water balance in a study area by employing the Water and Energy transfer Process in Large river basins (WEP-L), which is a physically-based distributed model. Khan *et al.* (2010) applied a global distributed hydrologic model, CREST, to the Nzoia basin, a sub-basin of Lake Victoria in the East Africa with semi-arid climate. They also assessed the applicability of multi-satellite remote sensing data, the Tropical Rainfall Measuring Mission (TRMM) Multi-satellite Precipitation Analysis (TMPA) products (Huffman *et al.*, 2007). Haddeland *et al.* (2011) compared results from six land surface models and five global hydrologic models in the Water Model Intercomparison Project (WaterMIP).

Prior to use of macroscale hydrologic models, the performance of each model must be evaluated and guaranteed at watershed scale based on reliable observation data. In this study, a distributed hydrologic model and remotely sensed precipitation dataset were evaluated and assessed in the Nakdong-River Basin in South Korea. The following sections of this report describe the methodology, introduce the selected hydrologic model and finally discuss the results from the model application to the target basins.

2. METHODOLOGY

The CREST model was used to evaluate the performance of a distributed hydrologic model with multi-satellite precipitation estimates, and five basins with multi-purpose

dams on the Nakdong-River, South Korea, were selected for its application. The TRMM 3B42 (*or* TMPA) products were applied to the hydrologic simulation as a meteorological forcing. Fig. 1 shows a schematic diagram relating the disparate parts of process, and the methods and datasets used in this study. Blue-colored parallelograms indicate raw datasets, blue rectangles represent estimated or generated data and red rectangles indicate methods, processes or models.

This section firstly gives a detailed description of the target basins. The processes involved in the generation of model inputs, including potential evapotranspiration and mean areal precipitation obtained from ground-based raingauges and a remotely sensed dataset is then described. Finally the topographical parameterization, obtained from digital elevation information and the distributed hydrologic model description are described in sequence.

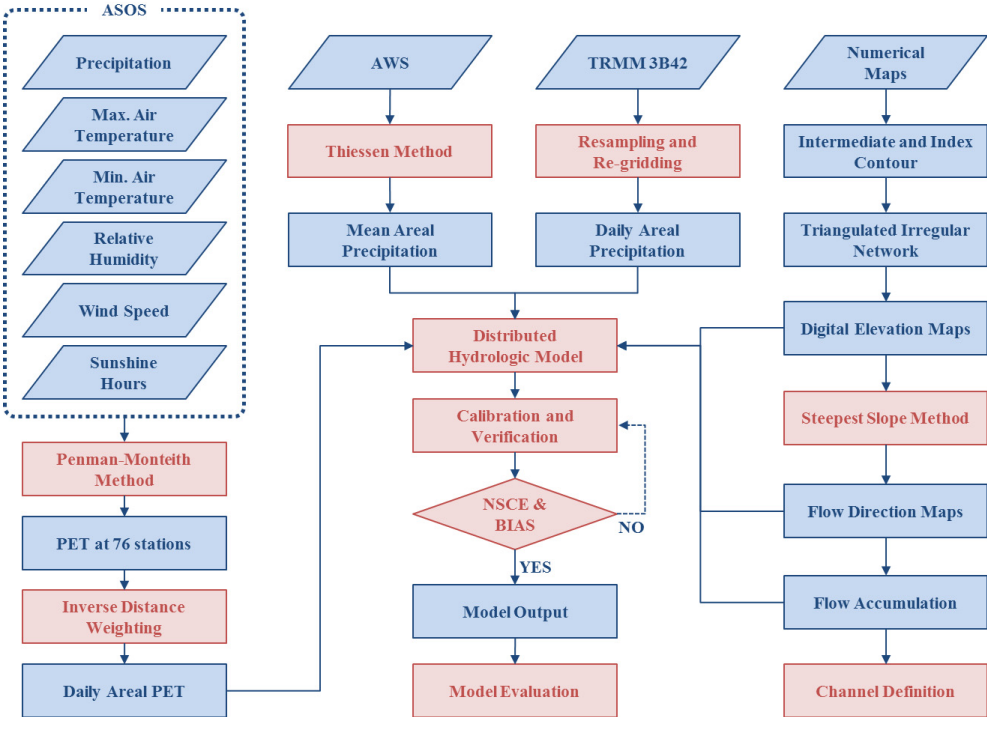

Figure 1 A schematic diagram of this study

2.1 Study Area

For this study we chose the Nakdong-River, located in the south-east Korean Peninsula (127°30′E-129°18′E, 34°58′N-37°14′N), with an extensive drainage area of approximately 23,702 km^2 (Fig. 2) and a main channel length of approximately 525.15 km. The Nakdong-River flows from the Hambaek Mountain to the South Sea and originates from a junction of the Hwangjicheon streams in Taebaek city, Gangwon province. The annual mean air temperature in the basin from 12°C to 14°C; annual mean precipitation is approximately 1231.4 mm, and annual mean runoff discharge is around 11,000,000,000 m^3.

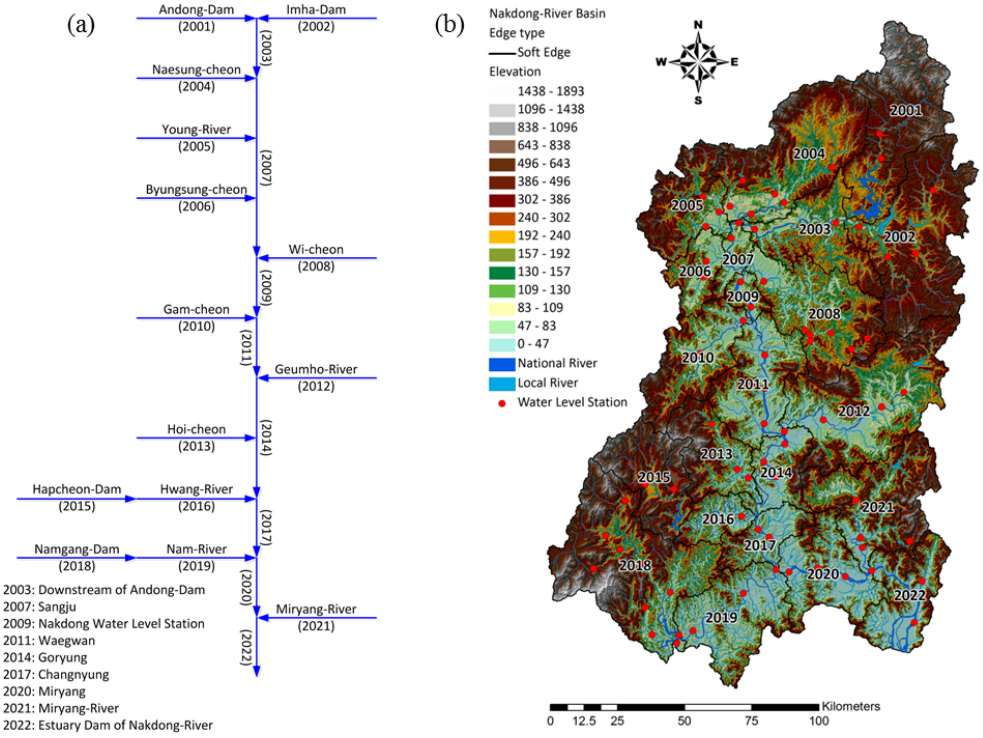

Figure 2 Diagram showing (a) the linkage structure of the basins and, (b) the digital elevation map and location of water level stations on the Nakdong River at South Korea

From 22 mid-scale basins within the river basin, we selected five basins with multi-purpose dams. They are as follows: the Andong-Dam Basin, the Imha-Dam Basin,

the Hapcheon-Dam Basin, the Namgang-Dam Basin and the Miryanggang-Dam Basin (Fig. 3). All are located in the upstream region of the river and the surrounding urban area is equal to or less than 1.1 percent of the size of each basin (Table 1); therefore, effects of artificial hydraulic structures and human activities are ignored in this hydrologic modeling.

Table 1 Physiographic attributes of the basins, rivers, multi-purpose dams, including land cover information within the target watersheds

	Attribute	Name of Basin				
		Andong-Dam	Imha-Dam	Hapcheon-Dam	Namgang-Dam	Miryanggang-Dam
Basin	Area (km^2)	1,628.7	1,975.8	928.9	2,293.4	1,975.8
	Perimeter (km)	272.1	320.2	188.8	328.0	320.2
	Mean Width (km)	9.5	17.5	14.5	20.6	17.5
	Mean Elevation (m)	549.3	388.4	504.6	426.3	388.4
	Mean Slope (%)	0.4	0.4	0.3	0.4	0.4
	Shape Factor	2.5	0.7	0.6	0.4	0.7
River	Length (km)	170.1	112.8	63.1	110.8	112.8
	Total Length (km)	5,381.9	5,741.6	3,352.6	6,866.6	5,741.6
	Upstream Elevation (m)	1,089.5	815.0	824.8	1,205.6	815.0
	Downstream Elevation (m)	96.3	89.0	128.7	39.2	89.0
Dam	Length (m)	612.0	515.0	472.0	1,126.0	535.0
	Height (m)	83.0	73.0	96.0	34.0	89.0
	Volume (103 m^3)	4,014.0	3,420.0	890.0	1,280.0	3,943.0
	Crest Elevation (m)	166.0	168.0	181.0	51.0	212.5
	Total Storage Capacity (106 m^3)	1,248.0	595.0	790.0	309.0	73.6
Land Cover	Water Area (%)	1.8	0.9	1.5	0.8	1.0
	Urbanization (%)	0.0	0.9	0.1	0.3	1.1
	Eroded Area (%)	0.5	0.4	0.2	0.1	0.4
	Marsh (%)	0.0	0.0	0.0	0.0	0.0
	Grassland (%)	0.0	0.0	0.0	0.0	0.0
	Forest (%)	85.5	81.6	76.5	78.2	74.8
	Paddy Field (%)	9.9	11.1	10.5	12.4	15.7
	Crop Land (%)	2.3	5.1	11.2	8.2	7.0

Fig. 2(a) is a schematic diagram relating the physical relationship between the basins on the Nakdong-River. Fig. 2(b) shows the digital elevation and location of water level stations in the river basin. Table 1 shows the attributes of basins, rivers, dams and land cover in the selected five basins.

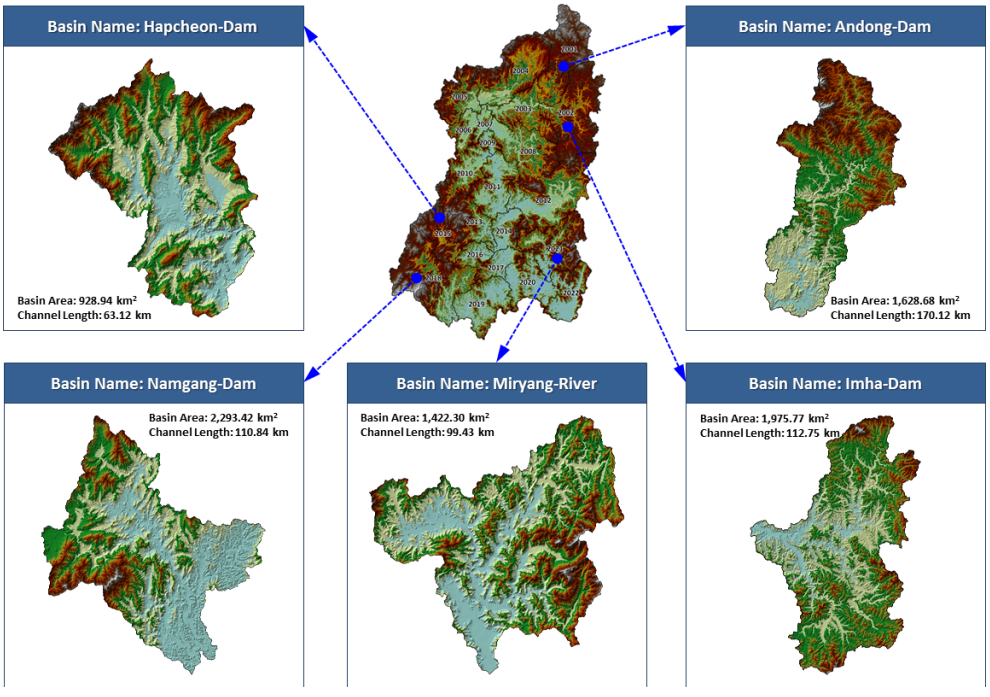

Figure 3 Location of the five basins selected for hydrological modeling

2.2 Meteorological Data

The CREST model requires only two meteorological forcing variables; precipitation and potential evapotranspiration.

A. Mean Areal Precipitation

The raingauge records for this study were supplied by Korea Hydro and Nuclear Power Corporation (KHNP), Korea Rural Community Corporation (KRCC), K-Water, Korea Meteorological Administration (KMA) and the Ministry of Land, Transport and Maritime Affairs, Republic of Korea. The Water Management Information System (WAMIS) integrates and provides these raingauge datasets through their web site (www.wamis.go.kr).

A distributed model such as the CREST model needs gridded input datasets of a certain resolution. However, surface precipitation data are measured at irregularly-scattered sites (where raingauges are installed) and it is very difficult to convert these datasets to gridded ones due to the spatial variability. In this study, therefore, we calculated and used the Mean Areal Precipitation (MAP) in a watershed (Fig. 4).

Methods such as the arithmetic average method, isohyetal method, and Thiessen's polygon method are used to convert data to MAP, and in this study we employed the most widely used Thiessen's polygon method. To compose Thiessen's polygons, the Delaunay triangulation is first performed among the raingauge points and the perpendicular at the midpoints of the three sides of the Delaunay triangles is then composed. When the Thiessen's polygons are completed, the MAP can be computed using Thiessen's equation.

$$\bar{P} = \sum_i P_i \frac{A_i}{A} \tag{1}$$

where, $\overline{P}$ is the MAP of the target basin; P_i, the precipitation at ith raingauge; A_i, the area of ith Thiessen's polygon; and A, the total area of the target basin.

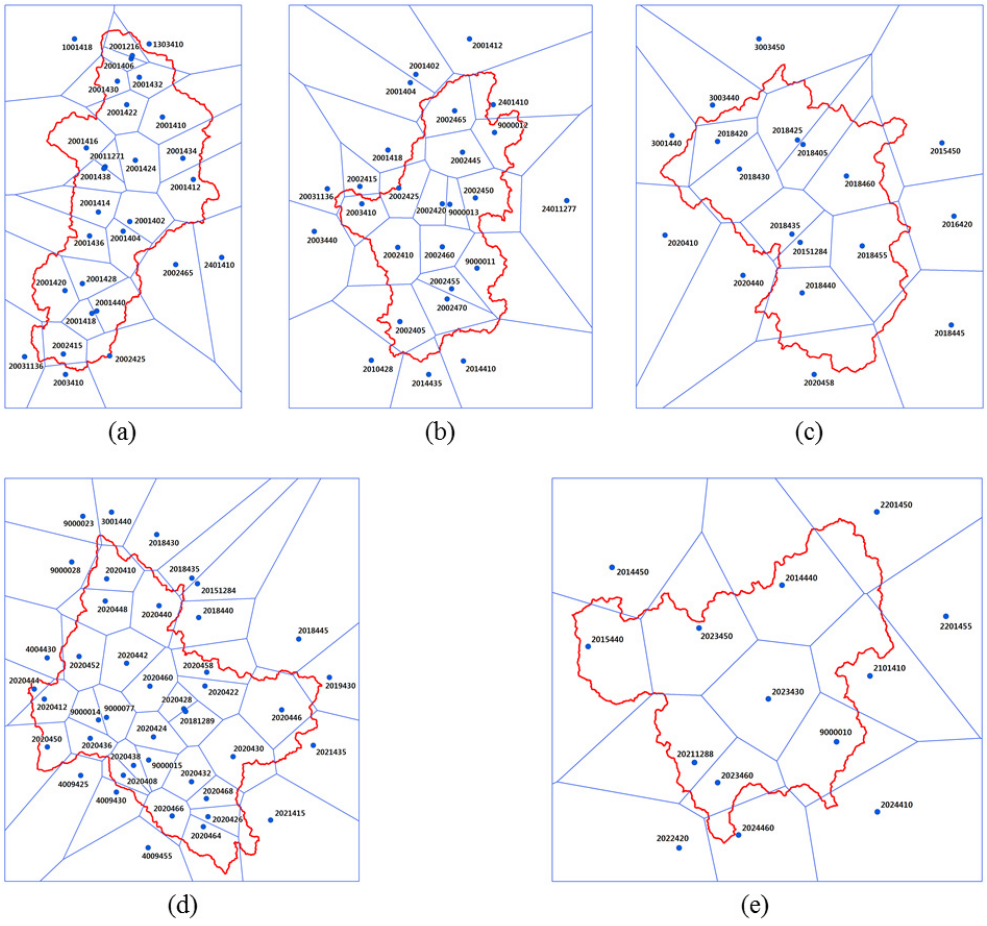

Figure 4 Thiessen's polygons for (a) the Andong-Dam Basin, (b) the Imha-Dam Basin, (c) the Hapcheon-Dam Basin, (d) the Namgang-Dam Basin, and (e) the Myranggang-Dam Basin

B. TMPA Products

Several multi-satellite based precipitation retrieval algorithms have been developed and used for operational and research purposes (Sorooshian *et al.*, 2000; Hong *et al.*, 2004; Joyce *et al.*, 2004; Huffman *et al.*, 2007). In this study, TRMM 3B42 V6 products from the National Aeronautics and Space Administration (NASA) were used as meteorological input forcing for the CREST model. The TMPA (TRMM

3B42) combined TRMM 2A12, Special Sensor Microwave Imager (SSMI), Advanced Microwave Scanning Radiometer - Earth observing system (AMSR-E) and Advanced Microwave Sounding Unit - B (AMSU-B) precipitation estimates. This provided precipitation estimates from multi-satellite datasets on a fine scale resolution, 3-hourly at 0.25° × 0.25° in both latitude and longitude, covering the globe from 50°S to 50°N (Huffman *et al.*, 2007).

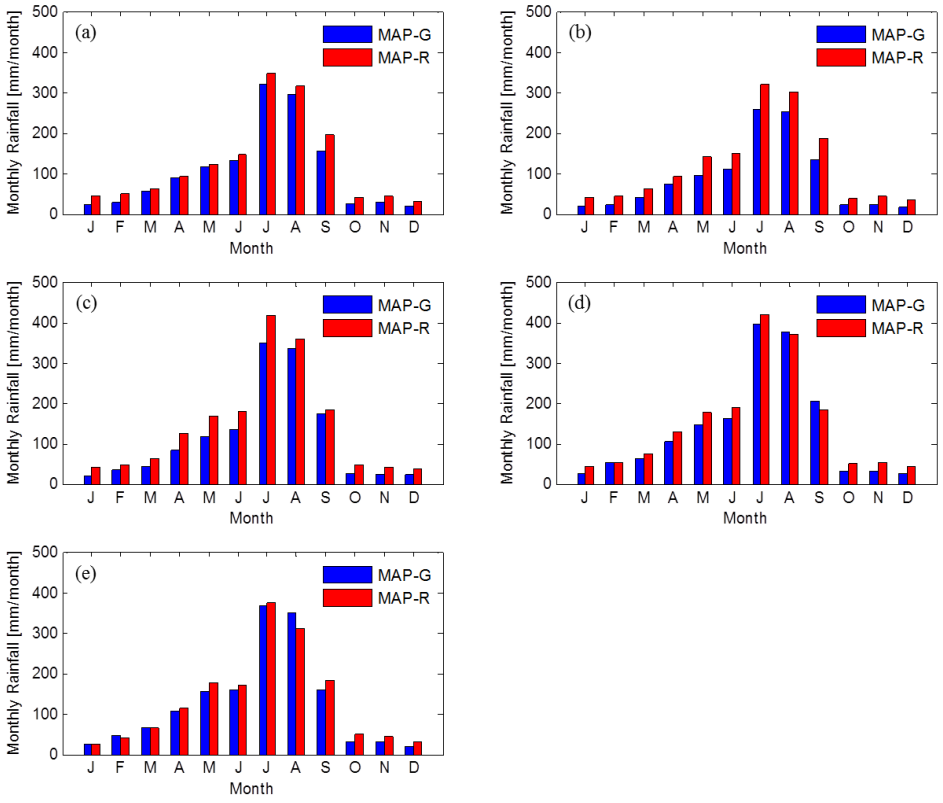

Figure 5 Bar diagrams comparing monthly MAP-G and MAP-R in the five basins

The global precipitation estimates from TMPA were resampled and regridded for the target area with a 1-km resolution. As mentioned above, the TMPA products have the spatial resolution of 0.25° (approximately 25 kilometers) and are relatively coarse resolution to be compared with a target basin area varying from 930 to 2300 km^2. Thus we used mean areal precipitation data computed from TMPA. The difference

between mean areal precipitation obtained from raingauges (MAP-G) and from remote sensing (MAP-R) were the analyzed. A comparison between monthly mean precipitation amounts demonstrated that between 2002 and 2010 the TMPA products overestimated the amounts throughout all seasons in the five target basins (Fig. 5).

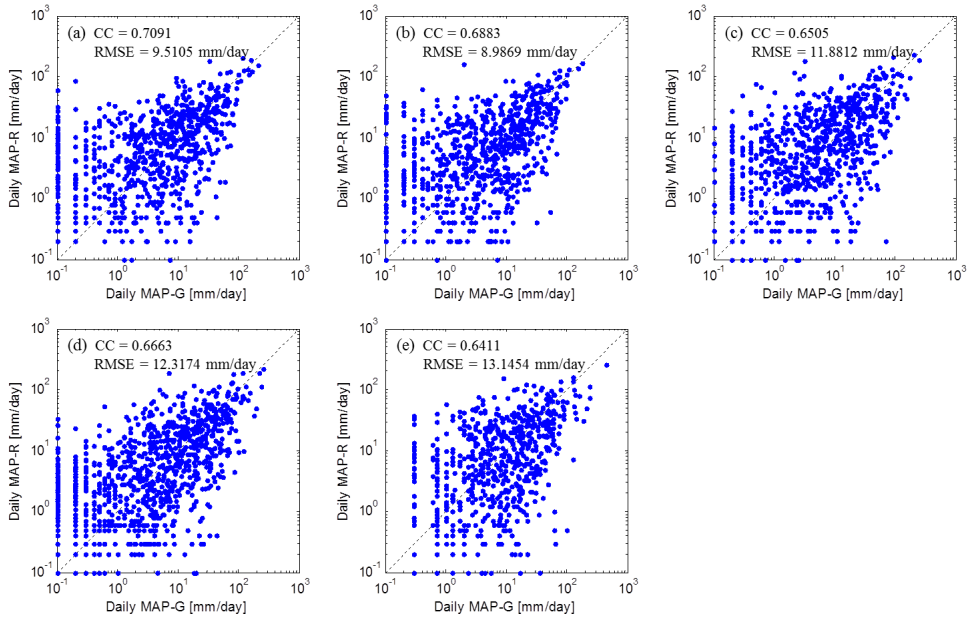

Figure 6 Scatterplots of the relationship between MAP-R and MAP-G in (a) the Andong-Dam Basin (CC = 0.7091, RMSE = 9.5105 mm/day), (b) the Imha-Dam Basin (CC = 0.6883, RMSE = 8.9869 mm/day), (c) the Hapcheon-Dam Basin (CC = 0.6505, RMSE = 11.8812 mm/day), (d) the Namgang-Dam Basin (CC = 0.6663, RMSE = 12.3174 mm/day) and (e) the Miranggang-Dam Basin (CC = 0.6411, RMSE = 13.1454 mm/day)

For example, from January to December in the Andong-Dam Basin (Fig. 5(a)), MAP-G reported 21.4mm, 27.6mm, 55.6mm, 90.0mm, 115.7mm, 132.4mm, 318.4mm, 295.8mm, 155.0mm, 24.5mm, 27.5mm and 18.4mm of monthly precipitation, respectively, whereas MAP-R reported 43.8mm, 50.2mm, 63.0mm, 93.4mm, 122.4mm, 147.7mm, 347.3mm, 315.3mm, 195.8mm, 42.1mm, 43.5mm and 31.4mm. This resulted in 104.7%, 81.8%, 13.3%, 3.8%, 5.8%, 11.6%, 9.1%, 6.6%, 26.4%, 72.2%, 58.4% and 70.1% more precipitation than MAP-G. This general trend is more noticeable during the cold season. Correlation coefficients between daily MAP-G and MAP-R in (a) the Andong-Dam Basin, (b) the Imha-Dam Basin, (c) the Hapcheon-Dam Basin,

(d) the Namgang-Dam Basin and (e) the Miryanggang-Dam Basin are respectively presented (Fig. 6). The scatterplots show that the correlation coefficients for each basin are 0.7091, 0.6883, 0.6505, 0.6663, 0.6411, and the root mean squared errors are 9.5105mm/day, 8.9869mm/day, 11.8812mm/day, 12.3174mm/day, and 13.1454mm/day, respectively.

C. Calculation of Potential evapotranspiration (PET)

A remotely sensed PET dataset is available from the Famine Early Warning Systems Network (FEWS NET) of the United States Geological Survey (USGS). However, the PET dataset has a spatial resolution of 1° (approximately 111 kilometers) and it is too coarse to be applied to a watershed scale modeling. For this study we computed the PET using weather observations.

To compute evapotranspiration we selected the Penman-Monteith equation from Food and Agriculture Organization (FAO) Paper 56 (Allen *et al.*, 1998). For the calculation of potential evapotranspiration using this equation, climatological measurements of sunshine hours, daily maximum and minimum air temperature, humidity and wind speed are needed.

Meteorological measurements were obtained from the 76 weather stations operated by the KMA (Table 2, Fig. 7(a)-7(e)) and the daily potential evapotranspiration at each weather stations was estimated during the period from 2002 to 2010 (Fig. 7(f)). The calculation procedures for potential evapotranspiration using the FAO Penman-Monteith equation are followed.

The FAO Penman-Monteith equation is given by

$$PET = \frac{0.408\Delta(R_n - G) + \gamma \frac{900}{T+273} u_2 (e_s - e_a)}{\Delta + \gamma(1 + 0.34u_2)} \quad (2)$$

where, PET is potential evapotranspiration[mm/day]; R_n, net radiation at the crop surface[$MJ/m^2/day$]; G, soil heat flux density[$MJ/m^2/day$];T, daily mean air

temperature at 2-m height[℃]; U_2, wind speed at 2-meter height[$m/\sec$]; e_s, saturated vapor pressure[kPa]; e_a, actual vapor pressure[kPa]; $(e_s - e_a)$, saturated vapor pressure deficit[kPa]; $\triangle$, slope vapor pressure curve[$kPa/℃$]; and , psychrometric constant[$kPa/℃$]. Each variable in the FAO Penman-Monteith equation is calculated using the following procedures;

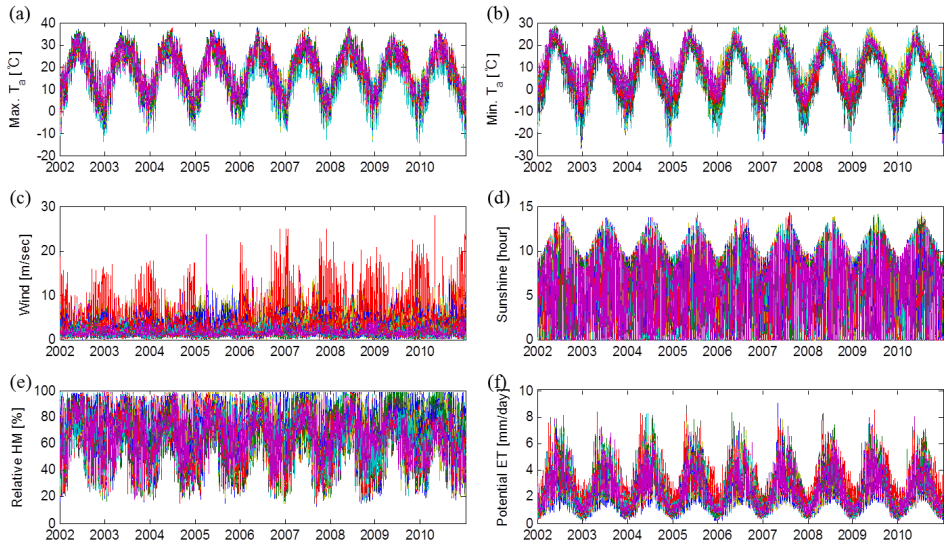

Figure 7 Daily time series of the meteorological variables at the KMA weather stations from 2002 to 2010, including daily: (a) maximum and (b) minimum air temperature, (c) wind speed, (d) sunshine hours, (e) relative humidity, and (f) estimated potential evapotranspiration

Daily mean air temperature, T [°C]

As in the equation below, mean air temperature is defined as the mean of the maximum and minimum air temperatures rather than as the average of hourly temperature measurements.

$$T = \frac{T_{min} + T_{max}}{2} \tag{3}$$

where, $T_{\min}$ is minimum air temperature [℃] and $T_{\max}$ is maximum air temperature [℃].

Vapor pressure deficit, $(e_s - e_a)[kPa]$

Vapor pressure deficit is defined as the difference between the saturated and actual vapor pressure.

Saturated vapor pressure, $e_s[kPa]$

Saturated vapor pressure is defined as the mean of the minimum and maximum vapor pressure:

$$e_s = \frac{e(T_{\min}) + e(T_{\max})}{2} \tag{4}$$

where,

$$e_{(T_{min})} = 0.6108\ exp\left(\frac{17.27\ T_{min}}{T_{min}+237.3}\right) \quad and \quad e_{(T_{max})} = 0.6108\ exp\left(\frac{17.27\ T_{max}}{T_{max}+237.3}\right) \tag{5}$$

Actual vapor pressure, $e_a[kPa]$

Actual vapor pressure is given by

$$e_a = 0.6108\ exp\left(\frac{17.27\ T_d}{T_d+237.3}\right) \quad or \quad e_a = \frac{RH_{mean}}{100}\left(\frac{e_{(T_{min})}+e_{(T_{max})}}{2}\right) \tag{6}$$

where, T_d is the dew point temperature[℃] and RH_{mean} is mean relative humidity[%].

Wind speed, $u_2[m/s]$

For the calculation of evapotranspiration, the measurement of wind speed at a 2-m height above the ground surface is required. If such 2-m measurements are not available but the height of anemometer is known, the wind speed should then be adjusted.

$$u_2 = u_y\left[\frac{4.87}{ln(67.8\ y-5.42)}\right] \tag{7}$$

where, y is the height of anemometer above the ground surface $[m]$;u_y , wind speed measurement at y meters above the surface $[m/s]$; and u_2, wind speed measurement

at 2-m above the ground $[m/s]$.

Net radiation, R_n [$MJ/m^2/day$]

Net radiation is computed by subtracting net long-wave radiation from net solar radiation.

$$R_n = R_{ns} - R_{nl} \tag{8}$$

where, R_n is net radiation $[MJ/m^2/day]$; R_{ns} , net solar radiation $[MJ/m^2/day]$; and R_{nl}, net long-wave radiation $[MJ/m^2/day]$.

Net solar radiation is estimated as follows:

$$R_{ns} = (1-\alpha)R_s \tag{9}$$

where, R_{ns} is net solar radiation $[MJ/m^2/day]$; , solar radiation $[MJ/m^2/day]$; and α, the albedo or canopy reflection coefficient, which is equal to 0.23 for the hypothetical reference crop.

Solar radiation is described by the following equation:

$$R_s = \left(0.25 + 0.50\frac{n}{N}\right) R_a \tag{10}$$

where, R_s is solar radiation $[MJ/m^2/day]$; n, the observed sunshine hours $[hour]$; R_a, extra-terrestrial radiation $[MJ/m^2/day]$; and N, the possible duration of sunshine hours $[hour]$.

$$N = \frac{24}{\pi}\omega_s \tag{11}$$

where, w_s is the sunset hour angle $[radian]$.

Slope vapor pressure curve, $\triangle$ [$kPa/℃$]

The slope of vapor pressure curve is given by the following equation.

$$\Delta = 4098 \times \left[\frac{0.6108 \exp\left(\frac{17.27T}{T+237.3}\right)}{(T+237.3)^2}\right] \quad (12)$$

where, $\triangle$ is the slope of vapor pressure curve at air temperature $T[kPa/℃]$.

Psychometric constant, γ [$kPa/℃$]

The psychometric constant is described by the following equation:

$$\gamma = \frac{c_p P}{\varepsilon \lambda} = 0.665 \times 10^{-3} P \quad (13)$$

where, γ is psychometric constant [$kPa/℃$]; λ, latent heat of vaporization which is equal to 2.45 [MJ/kg]; c_p, the specific heat at constant pressure (equal to 1.013×10^{-3} [$MJ/kg/℃$]); ε, the ratio between the molecular weight of water vapor and dry air (equal to 0.622); and P, atmospheric pressure [kPa].

The atmospheric pressure is given by the following equation:

$$P = 101.3\left(\frac{293 - 0.0065z}{293}\right)^{5.26} \quad (14)$$

where, z is the elevation above sea level [m].

Table 2 Location of weather stations used for the calculation of PET

Station	Latitude	Longitude	EL.m	Station	Latitude	Longitude	EL.m
Sokcho	38°15′	128°34′	22.9	Gosan	33°17′	126°09′	70.9
Cheorwon	38°09′	127°18′	154.9	Seongsan	33°23′	126°52′	18.4
Dongducheon	37°54′	127°04′	112.5	Seogwipo	33°14′	126°33′	50.4
Munsan	37°53′	126°45′	30	Jinju	35°09′	128°02′	27.1
Daegwallyeong	37°41′	128°43′	772.4	Ganghwa	37°42′	126°27′	46.1
Chuncheon	37°54′	127°44′	76.8	Yangpyeong	37°29′	127°30′	47.4
Baengnyeong-do	37°58′	124°38′	145.5	Icheon	37°16′	127°29′	90
Gangreung	37°45′	128°53′	26.1	Inje	38°04′	128°10′	198.7
Donghae	37°30′	129°07′	39.5	Hongcheon	37°41′	127°53′	146.2
Seoul	37°34′	126°57′	85.5	Taebaek	37°10′	128°59′	714.2
Incheon	37°29′	126°37′	54.6	Jecheon	37°09′	128°11′	263.1

Station	Latitude	Longitude	EL.m	Station	Latitude	Longitude	EL.m
Wonju	37°20′	127°57′	150.7	Boeun	36°29′	127°44′	173
Ulleung-do	37°30′	130°55′	222.5	Cheonan	36°46′	127°07′	21.3
Suwon	37°16′	126°59′	34.5	Boryeong	36°20′	126°33′	17.9
Yeongwol	37°11′	128°27′	239.7	Buyeo	36°16′	126°55′	11
Chungju	36°58′	127°57′	113.7	Geumsan	36°06′	127°29′	170.6
Seosan	36°47′	126°30′	25.2	Buan	35°43′	126°42′	3.6
Uljin	36°59′	129°25′	49.4	Imsil	35°36′	127°17′	248
Cheongju	36°38′	127°26′	56.4	Jeongeup	35°33′	126°52′	39.5
Daejeon	36°22′	127°22′	62.6	Namwon	35°24′	127°20′	89.7
Chupungryeong	36°13′	127°59′	242.2	Jangsu	35°39′	127°31′	407
Andong	36°34′	128°42′	140.7	Suncheon	35°04′	127°14′	74.4
Sangju	36°24′	128°09′	98	Jangheung	34°41′	126°55′	44.5
Pohang	36°02′	129°23′	1.3	Haenam	34°33′	126°34′	4.6
Gunsan	36°00′	126°45′	26.9	Goheung	34°37′	127°17′	62.8
Daegu	35°53′	128°37′	57.3	Bonghwa	36°56′	128°55′	320.9
Jeonju	35°49′	127°09′	61	Yeongju	36°52′	128°31′	210.5
Ulsan	35°33′	129°19′	34.6	Mungyeong	36°37′	128°09′	170.8
Masan	35°10′	128°34′	36.8	Yeongdeok	36°32′	129°25′	41.2
Gwangju	35°10′	126°53′	74.5	Uiseong	36°21′	128°41′	82.6
Busan	35°06′	129°02′	69.2	Gumi	36°07′	128°19′	47.4
Tongyeong	34°51′	128°26′	30.8	Yeongcheon	35°58′	128°57′	93.3
Mokpo	34°49′	126°23′	37.9	Geochang	35°40′	127°54′	221.4
Yeosu	34°44′	127°44′	73.3	Hapcheon	35°33′	128°10′	33
Heuksan-do	34°41′	125°27′	68.5	Miryang	35°29′	128°45′	10.7
Wan-do	34°23′	126°42′	27.7	Sancheong	35°24′	127°52′	138.7
Jin-do	34°28′	126°19′	476.4	Geoje	34°53′	128°36′	44.5
Jeju	33°30′	126°31′	19.9	Namhae	34°49′	127°56′	43.2

D. Discharge observations

For verification of hydrologic simulation, runoff discharge data are very essential. The Andong multi-purpose dam is located in the outlet part of the Andong-Dam Basin and other dams are also placed on the outlet of each basin except for the Miryanggang-Dam. So, we collected and utilized dam inflow observations from the WAMIS for model validation.

2.3 Topographic Parameterization

While lumped hydrologic models or semi-distributed hydrologic models use the mean value of basin properties such as slope, elevation, land cover and soil type in a basin or Hydrologic Response Units (HRUs), fully-distributed hydrologic models require the spatial distribution of these physical parameters. Digital Elevation Model (DEM) is most important in distributed hydrologic modeling, as the flow from one pixel to another is controlled by elevations at both pixels.

A. Elevation

Digital elevation can be generated from numerical maps. A numerical map includes information on topography, land use and artificial structures. In this study, after sampling both index and immediate contours from numerical maps, we composed a Triangulated Irregular Network (TIN). The TIN was then converted to DEM data for the target area.

B. Flow direction

Flow direction is generally defined as the direction of the steepest downhill gradient and can be determined by calculating the slope between a given pixel and eight neighboring pixels. The slope in each of these eight pixels is calculated using the difference in elevation indicated by the DEM value at every pixel (Fig. 8). This difference is then divided by the center-to-center distance between these pixels.

C. Flow accumulation

When the flow direction is assigned for each pixel, the flow accumulation at each pixel can then be computed (Fig. 9). The flow accumulation for a given pixel is defined as the number of upstream pixels or as the total area of upstream pixels

whose flow paths eventually pass through that pixel. Next, channel cells are defined as grid cells that exceed a flow accumulation threshold. In this study, we defined channel cells that have an upstream area of more than 30 km^2.

For this study, the above processes were applied to the Andong-Dam Basin (Fig. 10), the Imha-Dam Basin (Fig. 11), the Hapcheon-Dam Basin (Fig. 12), the Namgang-Dam Basin (Fig. 13) and the Miryanggang-Dam Basin (Fig. 14).

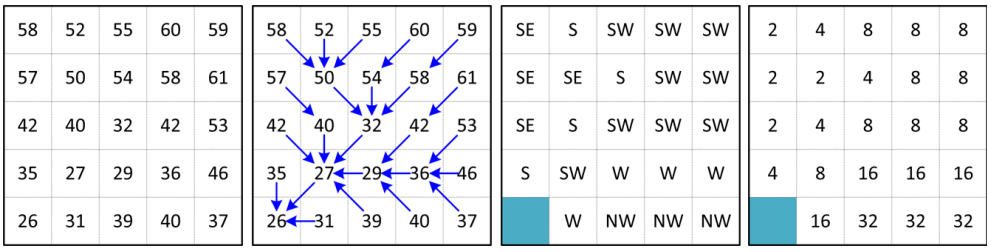

Figure 8 Conceptual diagrams for finding the flow direction using the steepest method

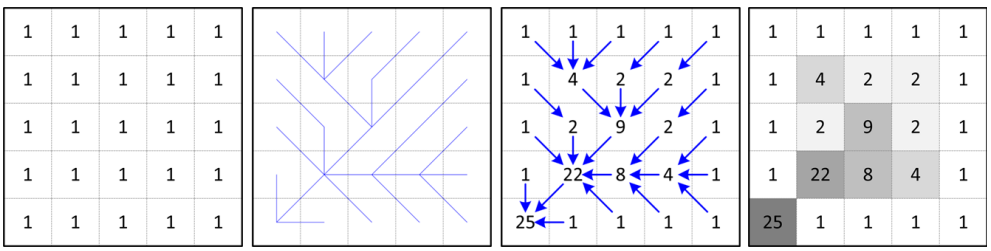

Figure 9 Conceptual diagrams for the calculation of flow accumulation

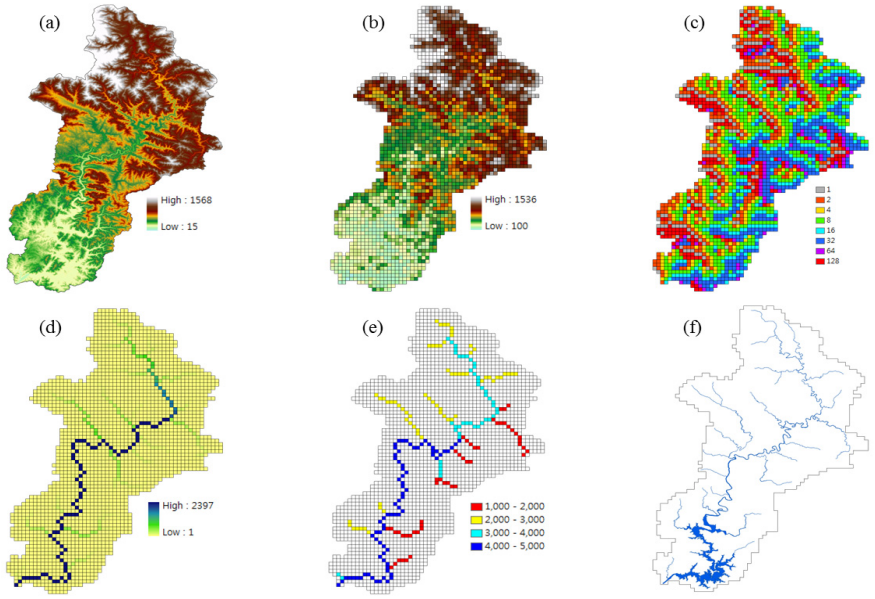

Figure 10 (a) 30-m DEM, (b) 1-km DEM, (c) flow direction map, (d) flow accumulation map, (e) channel cells, and (f) stream lines in the Andong-Dam Basin

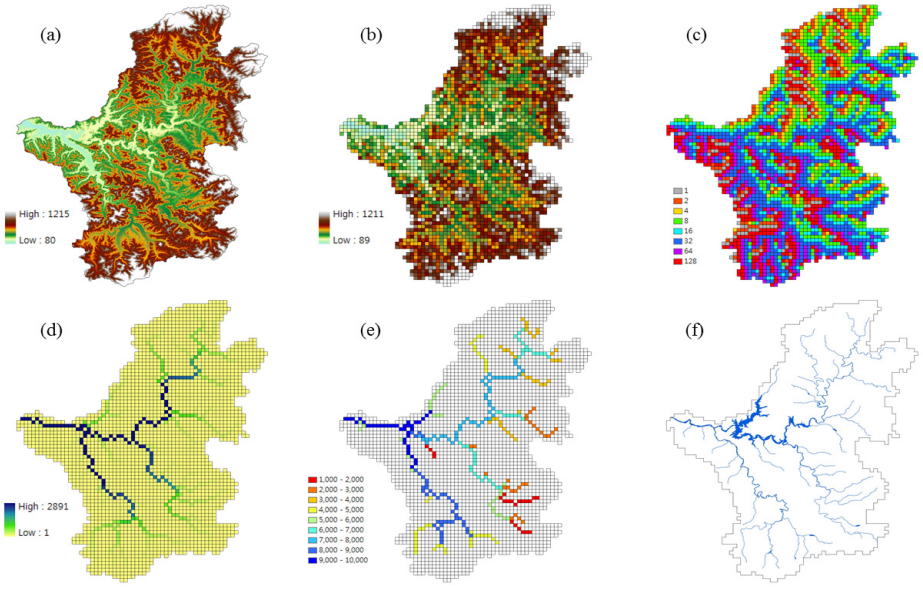

Figure 11 (a) 30-m DEM, (b) 1-km DEM, (c) flow direction map, (d) flow accumulation map, (e) channel cells, and (f) stream lines in the Imha-Dam Basin

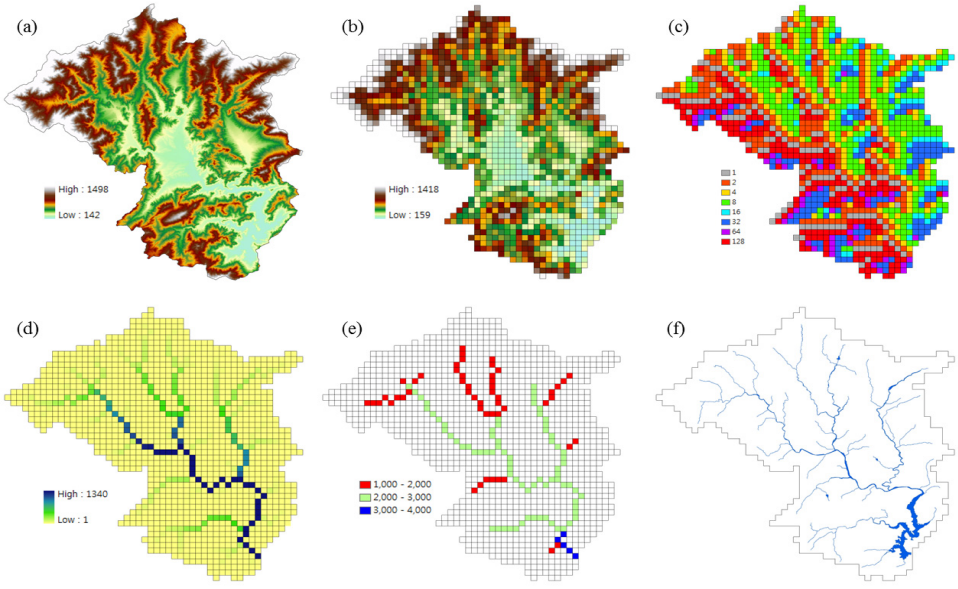

Figure 12 (a) 30-m DEM, (b) 1-km DEM, (c) flow direction map, (d) flow accumulation map, (e) channel cells, and (f) stream lines in the Hapcheon-Dam Basin

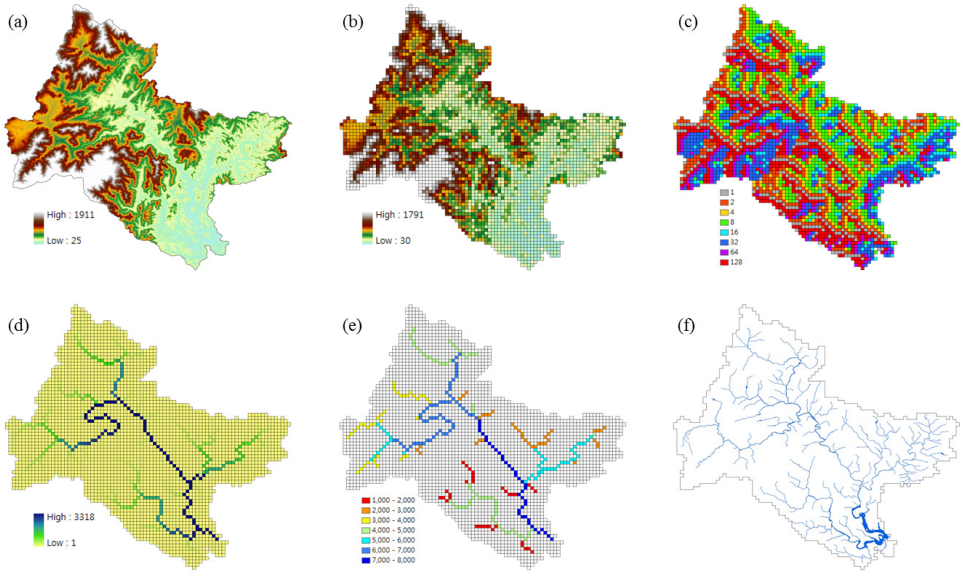

Figure 13 (a) 30-m DEM, (b) 1-km DEM, (c) flow direction map, (d) flow accumulation map, (e) channel cells, and (f) stream lines in the Namgang-Dam Basin

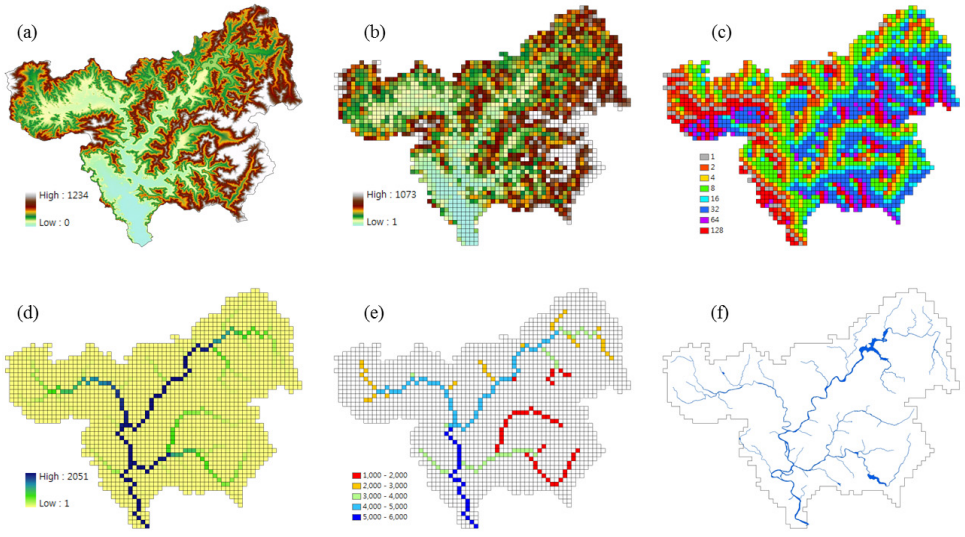

Figure 14 (a) 30-m DEM, (b) 1-km DEM, (c) flow direction map, (d) flow accumulation map, (e) channel cells, and (f) stream lines in the Miryanggang-Dam Basin

2.4 Distributed Hydrologic Model

The CREST model (Wang *et al.*, 2011), a distributed hydrologic model, was used to simulate streamflow in the Nakdong-River subbasins. The CREST model was developed by the University of Oklahoma in collaboration with the NASA SERVIR Project Team (www.servir.net). The model was initially developed for providing global flood predictions with a coarse resolution, but is also applicable to watershed scale modeling (Wang *et al.*, 2011). In this study, we focused on an evaluation of the model's performance on watershed scale. The CREST model consists of several core components; rainfall-runoff generation, evapotranspiration, sub-grid cell routing, downstream routing and feedback between the routing and rainfall-runoff modules (Fig. 15). A description of the model follows:

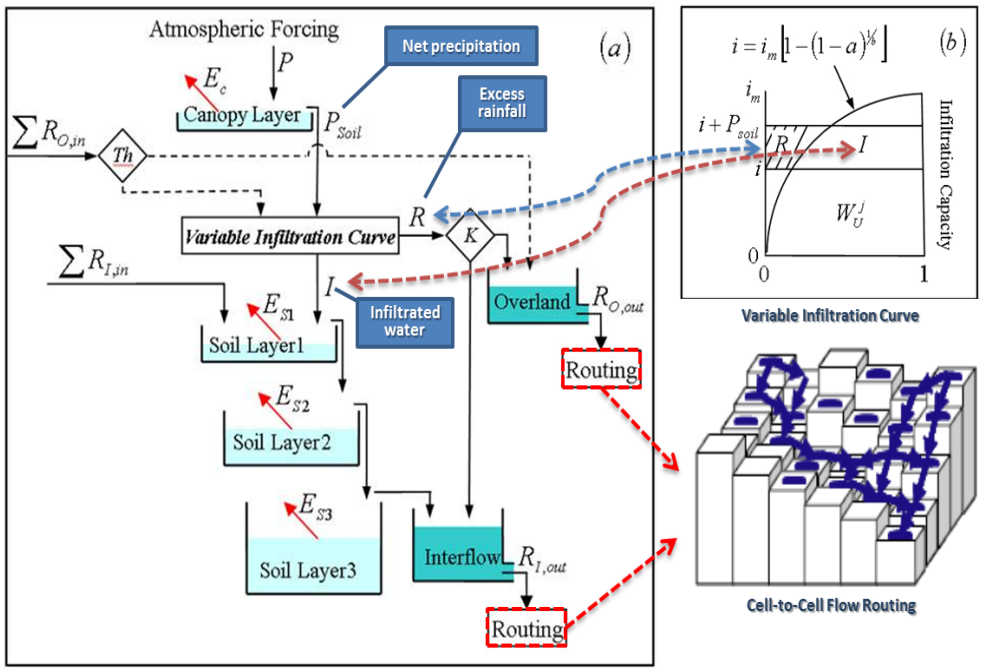

Figure 15 Hydrological processes delineated in the CREST model (Wang *et al.*, 2011)

A. Interception

When a precipitation event occurs, a fraction of the precipitation is intercepted by the vegetation canopy and an excess storage reservoir was employed to simulate this process. The maximum storage capacity of the reservoir is defined by the canopy interception capacity (CIC).

$$CIC = k_c \times d \times LAI \tag{15}$$

where, k_c is the coefficient of the land cover's CIC;d, the vegetation coverage, and LAI, the leaf area index.

The amount of precipitation reduced by interception becomes net precipitation. A portion of this net precipitation will fall on the land surface.

$$P_{soil} = P - (CIC - CI) \tag{16}$$

where, P_{soil} is the precipitation reaching the soil surface, and CI is the depth of the water intercepted by the vegetation canopy.

B. Infiltration

The precipitation reaching the soil surface is divided into excess rainfall and infiltration water according to the Variable Infiltration Curve (VIC), founded in the Xinanjiang model (Zhao, 1992). The curve is given as follows:

$$i = i_m \left[1 - \left(1 - \frac{W}{W_m}\right)^{\frac{1}{1+b_i}}\right] \tag{17}$$

where, i is the point infiltration capacity;i_m, the maximum infiltration capacity of a cell; W_m, the maximum water capacity; W, the total mean water of the three soil layers; and b_i, the exponent of the curve. The amount of infiltration water is computed as follows:

$$\text{for } i + P_{soil} \geq i_m,$$

$$I = (W_m - W) \tag{18}$$

for $i + P_{soil} < i_m$,

$$I = (W_m - W) + W_m (1 - \frac{i + P_{soil}}{i_m})^{1+b_i} \quad (19)$$

This model employed three storage reservoirs representing three different soil layers. Infiltration water firstly enters the upper soil layer until it is saturated. The middle and lower layers are then filled in sequence.

C. Runoff generation

The remaining net precipitation, with the exception of the infiltration water, is the excess rainfall, and can be calculated as follows:

$$R = P_{soil} - I \quad (20)$$

The excess rainfall is then divided again into overland excess rain and interflow excess rain according to relationship between net precipitation and the infiltration rate of the upper layer.

for $P_{soil} > K$

$$R_I = K\frac{R}{P_{soil}}, \; R_o = R - R_I \quad (21)$$

for $P_{soil} \leq K$

$$R_I = R, \; R_o = 0 \quad (22)$$

where, K is closely related to the saturated hydraulic conductivity of the soil.

D. Evapotranspiration

The process of evapotranspiration removes water from the canopy reservoir and continues until this reservoir is completely depleted.

for $CI > E_p$

$$E_c = E_p \tag{23}$$

for $CI \leq E_p$

$$E_c = CI \tag{24}$$

where, E_c is the water removed from the canopy layer. The potential evapotranspiration in the upper soil layer is computed as follows:

$$E_{p1} = E_p - E_c \tag{25}$$

The rate of water removed from the upper soil layer is computed as follows:

for $W_1 > E_{p1}$

$$E_{s1} = E_{p1} \tag{26}$$

for $W_1 \leq E_{p1}$

$$E_{s1} = W_1 \tag{27}$$

where, W_1 indicates the water depth in the upper soil layer reservoir. The potential evapotranspiration in the middle soil layer is calculated as follows:

$$E_{p2} = (E_{p1} - E_{s1})\sqrt{\frac{W_2}{W_{m2}}} \tag{28}$$

The rate of water evaporated from the middle soil layer is computed as follows:

for $W_2 > E_{p2}$

$$E_{s2} = E_{p2} \tag{29}$$

for $W_2 \leq E_{p2}$

$$E_{s2} = W_2 \tag{30}$$

where, W_2 indicates the water depth in the middle soil layer reservoir. The potential evapotranspiration in the lower soil layer is computed as follows:

$$E_{p3} = \left(E_{p2} - E_{s2}\right)\frac{W_3}{W_{m3}} \tag{31}$$

The rate of water evaporated from the lower soil layer is computed as follows:

for $W_3 > E_{p3}$

$$E_{s3} = E_{p3} \tag{32}$$

for $W_3 \leq E_{p3}$

$$E_{s3} = W_3 \tag{33}$$

where, W_3 indicates the water depth in the reservoir in the lower soil layer. The total evaporated water from the three layers is thus computed as follows:

$$E_a = E_c + E_{s1} + E_{s2} + E_{s3} \tag{34}$$

E. Sub-grid-scale routing

Two linear reservoir models are employed to simulate sub-grid cell routing in the CREST model. Overland and interflow excess rainfall enters the two reservoirs separately and the water depth of the two reservoirs is computed as follows:

$$S_{o,\,t+1} = S_{o,\,t} + R_{o,\,t} \tag{35}$$

$$S_{I,\,t+1} = S_{I,\,t} + R_{I,\,t} \tag{36}$$

where, S_o and S_I are the overland and interflow reservoir depth separately and the subscript t is the time step. The runoff discharge from the overland and interflow reservoirs is computed as follows:

$$R_o = K_o \times S_o \tag{37}$$

$$R_I = K_I \times S_I \tag{38}$$

where, K_o and K_I are the overland and interflow reservoir discharge parameters, which are a function of the watershed characteristics such as basin area and slope.

F. Downstream routing

The concentration time for overland and interflow runoff is computed as follows:

$$T^j = \frac{l^j}{K_x \sqrt{S^j}} \tag{39}$$

where, the subscript j refers to the spatial index of a cell; T^j, the concentration time from the jth cell to its downstream $(j+1)$th cell; l^j, the distance between the centers of the jth cell to the $(j+1)$th cells; S^j, the slope from the jth cell to the $(j+1)$th cell; and K_X, the runoff velocity coefficient corresponding to the land surface roughness.

G. Water balance calculation for each cell

The water balance at a given cell is calculated as follows:

$$\frac{dS}{dt} = P - E_a + \sum Q_{O,in} - Q_{O,out} + \sum Q_{I,in} - Q_{I,out} \tag{40}$$

where, S is the total water storage in each cell and the subscript O and I indicate the overland and interflow.

H. Consideration of the impact of precipitation and upstream cell

Since routed water from a cell impacts both rainfall-runoff generation and the routing, these processes are needed to couple each other. Overland runoff from upstream cells is assumed that net precipitation is added to the upper soil layer. Net precipitation is thus adjusted as follows:

$$\hat{P}_{soil} = P_{soil} + \sum_i Q_{O,i} \tag{41}$$

where, $\hat{P}_{soil}$ is the adjusted P_{soil} as dictated by the total amount of overland runoff from upstream cells. Soil moisture content is increased by the lateral inflow coming from upstream cells. Thus, the amount of infiltrated water is adjusted as follows:

$$\hat{I} = I + \sum_i Q_{I,i} \tag{42}$$

where, $\hat{I}$ is the adjusted I determined by the sum of the interflow from upstream cells. Finally, channel runoff from upstream cells contributes to the overland reservoir depth. Thus, the total water storage is adjusted as follows:

$$\hat{S}_O^{t+1} = S_O^t + R_O^t + \sum Q_{O,in} \tag{43}$$

where, $\hat{S}_O^{t+1}$ is the adjusted S_O^{t+1} increased by upstream channel cells.

2.5 Model Calibration

The CREST model provides an automatic calibration routine based on an Adaptive Random Search (ARS) method (Brooks, 1958). The two most commonly used indicators, the Nash-Sutcliffe Coefficient of Efficiency (NSCE) (Nash and Sutcliffe, 1970) and the relative bias ratio, were applied to the calibration (a detailed description of these indices will be given in the following section). These indicators were used as objective functions for the calibration. The CREST model includes many parameters, which require optimization (Table 3).

Table 3 Model parameters requiring optimization (Wang *et al.*, 2011)

Parameter Description	Default	Unit
Exponent of variable infiltration curve	0.2	-
Coefficient of land cover's CIC	0.5	-
Interflow reservoir discharge parameter	0.1	-
Overland reservoir discharge parameter	0.5	-
Runoff velocity coefficient (Varies in overland, channel and interflow)	50/100/15	-

Parameter Description	Default	Unit
Threshold between overland and channel	30	km^2
Maximum cell water capacity of 1st soil layer	20	mm
Maximum cell water capacity of 2nd soil layer	50	mm
Maximum cell water capacity of 3rd soil layer	80	mm

2.6 Model Evaluation

The performance of the model was assessed using four common statistical indices. The NSCE is a normalized statistic that determines the relative magnitude of the noise compared to the variance of the measurements. We therefore employed the NSCE for the investigation of the statistical goodness-of-fit of simulated discharge. The NSCE is computed as follows:

$$NSCE = 1 - \frac{\Sigma_i \left(Q_{obs}^i - Q_{sim}^i\right)^2}{\Sigma_i (Q_{obs}^i - \bar{Q}_{obs})^2} \quad (44)$$

where, the subscript i indicates the th day of discharge time series. Q_{obs} and Q_{sim} are the observed and simulated discharges. $\bar{Q_{obs}}$ is the average of all the observed discharges. The NSCE varies from negative infinity to one and the model provides the best results when NSCE is equal to one. The systematic bias of the simulated discharge was assessed using the percent bias (or relative bias ratio) as follows:

$$BIAS = \frac{\Sigma_i Q_{obs}^i - \Sigma_i Q_{sim}^i}{\Sigma_i Q_{obs}^i} \times 100(\%) \quad (45)$$

Positive and negative values indicate an underestimation and overestimation respectively (Gupta *et al.*, 1999). To evaluate a hydrologic model, Singh *et al.* (2005) developed and proposed the Root Mean Squared Error (RMSE) – Observations Standard Deviation Ratio (RSR).

$$RSR = \frac{\sqrt{\Sigma_i (Q_{obs}^i - Q_{sim}^i)^2}}{\sqrt{\Sigma_i (Q_{obs}^i - \bar{Q}_{obs})^2}} \quad (46)$$

RSR is the standardized RMSE using the standard deviation of the measurements (Moriasi *et al.*, 2007). It varies from the optimal value of zero to a large positive value. Finally, the Pearson's Correlation Coefficient (PCC) is used to assess the collinearity between simulated and observed discharge series.

$$PCC = \frac{\Sigma_i\left(Q_{obs}^i - \bar{Q}_{obs}\right)\left(Q_{sim}^i - \bar{Q}_{sim}\right)}{\sqrt{\Sigma_i\left(Q_{obs}^i - \bar{Q}_{obs}\right)^2\left(Q_{sim}^i - \bar{Q}_{sim}\right)^2}} \quad (47)$$

where, $\bar{Q}_{sim}$ is the average of all the simulated discharge. The best model performance occurs when NSCE = 1, BIAS = 0(%), RSR = 0 and PCC = 1.

Moriasi *et al.* (2007) recommended model evaluation techniques including statistical and graphical skills and proposed criteria for model evaluation in terms of the accuracy of simulated streamflow compared to the observed data (Table 4). We attempted to evaluate a distributed hydrologic model using these performance ratings.

Table 4 General performance ratings for streamflow simulation in a monthly time-step

Performance Rating	NSCE	BIAS	RSR
Very Good	0.75 < NSCE ≤ 1.00	BIAS < ±10	0.00 ≤ RSR ≤ 0.50
Good	0.65 < NSCE ≤ 0.75	±10 ≤ BIAS < ±15	0.50 < RSR ≤ 0.60
Satisfactory	0.50 < NSCE ≤ 0.65	±15 ≤ BIAS < ±25	0.60 < RSR ≤ 0.70
Unsatisfactory	NSCE ≤ 0.50	BIAS ≥ ±25	RSR > 0.70

3. RESULTS

The CREST was implemented at a 1-km resolution for every target basin and driven by daily precipitation obtained from raingauges and multisatellite datasets. The CREST model was calibrated by daily-observed dam inflow data from 2002/01/01 to 2004/12/31 and validated for the period 2005/01/01 and 2011/12/31. Model parameters were adjusted during the calibration period and then fixed, and the simulation of streamflow during the validation period was then implemented. Monthly hydrographs (from Fig. 16 to Fig. 20) represent the comparison between the observed dam inflow and the simulation results from different mean areal precipitation datasets estimated from raingauges and from TMPA for each basin.

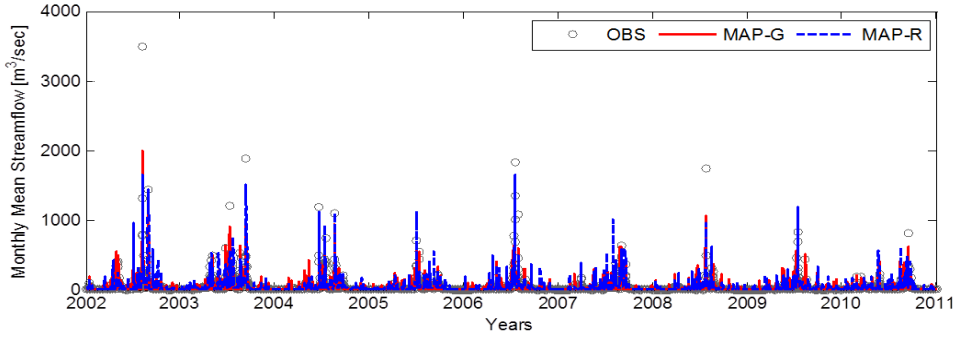

Figure 16 Comparison hydrographs of monthly mean observed dam inflow (OBS) and simulated inflow using raingauge records (MAP-G) and TRMM 3B42 (MAP-R) in the Andong-Dam Basin

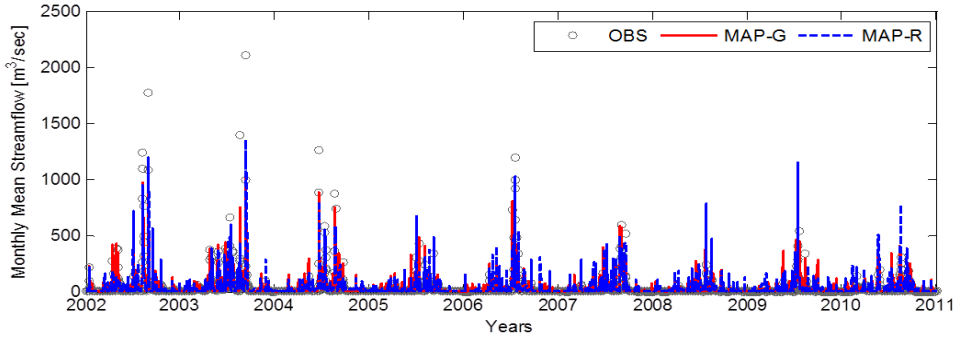

Figure 17 Comparison hydrographs of monthly mean observed dam inflow (OBS) and simulated inflow using raingauge records (MAP-G) and TRMM 3B42 (MAP-R) in the Imha-Dam Basin

Table 5 and 6 shows the summary statistics in daily time-step for the simulation using MAP-G and MAP-R respectively. Table 7 and 8 present the simulation results for monthly time-step using MAP-G and MAP-R. We focus on and discuss the results in the monthly time-step using Table 4.

The CREST model shows a “very good” performance using MAP-G during both the calibration (NSCE = 0.9272, BIAS = -0.2718, RSR = 0.2698 and PCC = 0.9691) and validation period (NSCE = 0.8363, BIAS = -1.4407, RSR = 0.4046 and PCC = 0.9258) in the Andong-Dam Basin (Table 4 and 7). The CREST modeling using MAP-G also generated the simulated streamflow timeseries with “very good” ratings during the calibration period in all other basins. However, in the Imha-Dam and Miryanggang-Dam Basin, only “good” scores were obtained during the model validation period in comparison with the observations. These results indicate that the CREST model using MAP-G can adequately simulate the discharge in the five target basins.

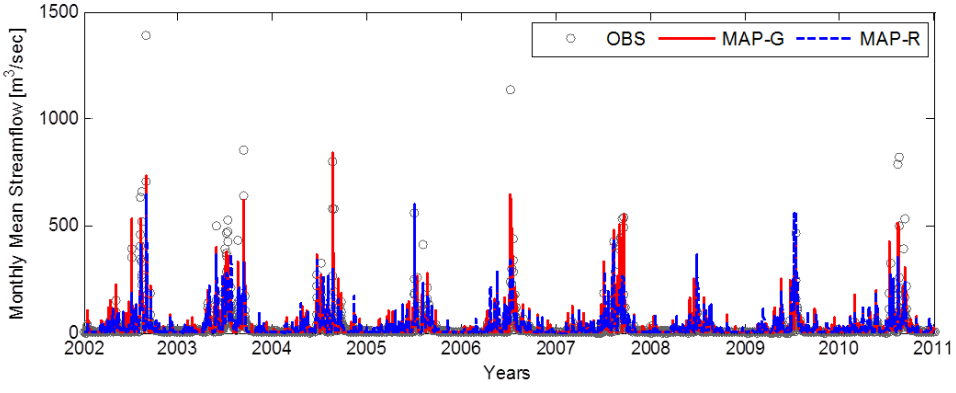

Figure 18 Comparison hydrographs of monthly mean observed dam inflow (OBS) and simulated inflow with raingauge records (MAP-G) and TRMM 3B42 (MAP-R) in the Hapcheon Basin

In comparison with the streamflow simulation using MAP-G, the results using MAP-R are relatively unsatisfactory, according to the summary statistics (Table 8). For example, in the Imha-Dam Basin, the parameters appeared to be well calibrated with NSCE = 0.8271, BIAS = -0.4088, RSR = 0.4159 and PCC = 0.9180 during the calibration period. However, during the validation period the CREST model generated a very poor result: NSCE = 0.4482, BIAS = -3.7460, RSR = 0.7428 and PCC = 0.9003.

This result would be expected to originate errors between daily precipitation amounts computed from raingauges and those from remotely sensed datasets.

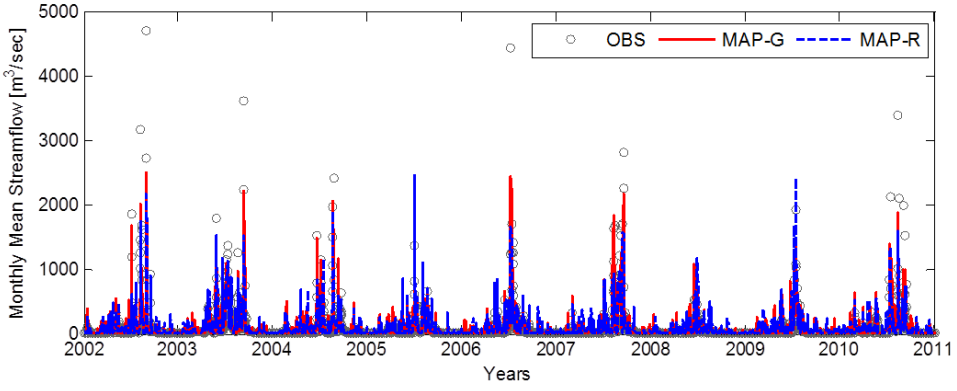

Figure 19 Comparison hydrographs of monthly mean observed dam inflow (OBS) and simulated inflow with raingauge records (MAP-G) and TRMM 3B42 (MAP-R) in the Namgang-Dam Basin

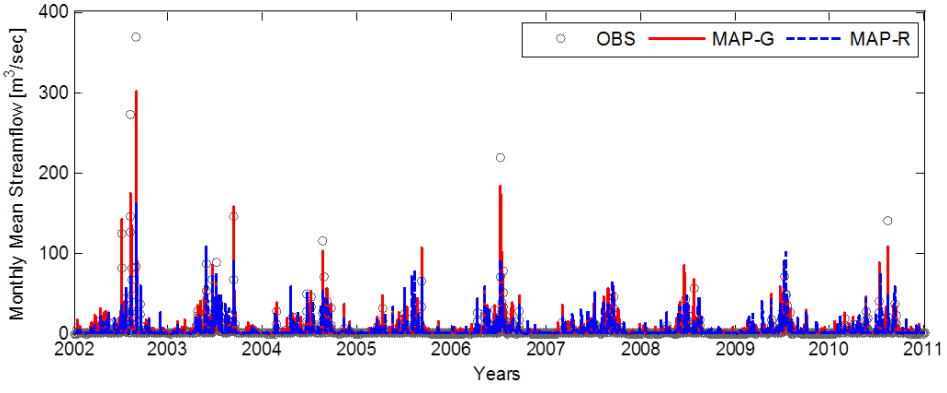

Figure 20 Comparison hydrographs of monthly mean observed dam inflow (OBS) and simulated inflow with raingauge records (MAP-G) and TRMM 3B42 (MAP-R) in the Mirayngang-Dam Basin

Table 5 Summary statistics for daily time-step for the simulation using MAP-G

Basin Name	Calibration Period				Validation Period			
	NSCE	BIAS	RSR	PCC	NSCE	BIAS	RSR	PCC
Andong-Dam	0.7693	-8.1854	0.4803	0.8775	0.5684	-43.8810	0.6570	0.7897
Imha-Dam	0.7152	-17.6547	0.5337	0.8480	0.3430	-105.6225	0.8106	0.7762
Hapcheon-Dam	0.8042	-8.2866	0.4425	0.8974	0.6910	-42.0252	0.5559	0.8539
Namgang-Dam	0.8049	-19.7152	0.4417	0.9001	0.7049	-44.2060	0.5432	0.8524
Miryanggang-Dam	0.8714	-19.3757	0.3587	0.9348	0.4850	-66.3840	0.7177	0.8274

Table 6 Summary statistics for daily time-step for the simulation using MAP-R

Basin Name	Calibration Period				Validation Period			
	NSCE	BIAS	RSR	PCC	NSCE	BIAS	RSR	PCC
Andong-Dam	0.6888	-10.5254	0.5578	0.8308	0.4423	-58.0637	0.7468	0.7616
Imha-Dam	0.5662	-12.3325	0.6586	0.7542	-0.1722	-114.3419	1.0827	0.6468
Hapcheon-Dam	0.5233	-10.9799	0.6904	0.7252	0.2415	-61.9059	0.8709	0.6173
Namgang-Dam	0.6210	-14.4284	0.6156	0.7913	0.3816	-56.1900	0.7864	0.6850
Miryanggang-Dam	0.4705	-12.8742	0.7276	0.6873	-0.1260	-91.5288	1.0611	0.5771

Table 7 Summary statistics for monthly time-step for the simulation using MAP-G

Basin Name	Calibration Period				Validation Period			
	NSCE	BIAS	RSR	PCC	NSCE	BIAS	RSR	PCC
Andong-Dam	0.9272	-0.2718	0.2698	0.9691	0.8363	-1.4407	0.4046	0.9470
Imha-Dam	0.9102	-0.5799	0.2997	0.9635	0.5291	-3.4568	0.6863	0.9258
Hapcheon-Dam	0.9283	-0.2755	0.2679	0.9678	0.8471	-1.3777	0.3910	0.9511
Namgang-Dam	0.8974	-0.6530	0.3203	0.9639	0.8467	-1.4538	0.3916	0.9510
Miryanggang-Dam	0.9585	-0.6393	0.2038	0.9884	0.6906	-2.1773	0.5562	0.9488

Table 8 Summary statistics for monthly time-step for the simulation using MAP-R

Basin Name	Calibration Period				Validation Period			
	NSCE	BIAS	RSR	PCC	NSCE	BIAS	RSR	PCC
Andong-Dam	0.8404	-0.3529	0.3995	0.9269	0.7831	-1.9056	0.4658	0.9435
Imha-Dam	0.8271	-0.4088	0.4159	0.9180	0.4482	-3.7460	0.7428	0.9003
Hapcheon-Dam	0.8116	-0.3696	0.4341	0.9105	0.4750	-2.0217	0.7246	0.8037
Namgang-Dam	0.7875	-0.4811	0.4610	0.9015	0.6548	-1.8385	0.5876	0.8648
Miryanggang-Dam	0.6535	-0.4341	0.5886	0.8149	0.3460	-2.9965	0.8087	0.8969

4. SUMMARY AND CONCLUSION

In this study we evaluated the CREST model and investigated the applicability of satellite-based precipitation estimates. Prior to a streamflow simulation using this model, mean areal precipitation datasets using both raingauges and multisatellite precipitation estimates were generated as MAP-G and MAP-R. A simple comparison of them was also presented with a correlation coefficient and root mean squared error. The CREST model was then implemented in five sub-basins on the Nakdong-River at a 1-km spatial resolution and then daily time-step. The model calibrated from 2002 to 2004 and then validated from 2005 and 2010 using the ARS method embedded in the hydrologic model. Finally, the model's performance was evaluated using four common statistics including NSCE, BIAS, RSR, and PCC.

The results showed that MAP-R tended to provide overestimates than MAP-G during the whole season and this general trend increased during the cold season. Considering the correlation coefficients, which varied from 0.6411 to 0.7091 and the root mean squared errors, which varied from 8.9869 mm/day to 13.1454 mm/day, the relationship between MAP-R and MAP-G in each basin appeared to be slightly weak. These results are expected to originate from the present limitations of remote sensing techniques, such as differences in temporal and spatial resolution, the selection of representative value and different microwaves attenuations.

The results from the simulation using MAP-G, during both the calibration and validation period, indicate that this hydrologic model can effectively simulate the streamflow in the target basins, and that it gives very good performance. This indicates that the model can be applied to predict runoff discharge in other basins with different attributes such as different drainage area, elevation, slope, land cover and soil type. However, the hydrological simulation using MAP-R provided unsatisfactory results during the validation period in all five basins.

We have identified that the CREST model predicts streamflow very well and that the satellite-based precipitation estimates contain errors, which affect the

hydrological simulation throughout this study. However, it is clear that remote sensing data are useful for hydrological modeling. It is believed that in the near future the development of new satellites and the use of statistical correction will increase the utility of satellite precipitation estimates, and these datasets will promote the applicability and accuracy of hydrological simulations.

REFERENCES

Alcamo, J., P. Döll, T. Henriches, F. Kaspar, B. Lehner, T. Rösch, and S. Siebert, 2003: Development and testing of the WaterGAP 2 global model of water use and availability. *Hydrological Sciences Journal*, 48(3), 317-337.

Allen, R. G., L. S. Pereira, D. Raes, and M. Smith, 1998: Crop evapotranspiration – Guidelines for computing crop water requirements. *FAO Irrigation and drainage paper 56*, Rome, Italy: Food and Agriculture Organization of the United Nations, ISBN 92-5-104219-5.

As-Syakur, A. R., T. Tanaka, R. Prasetia, I. K. Swardika, and I. W. Kasa, 2011: Comparison of TRMM Multisatellite Precipitation Analysis (TMPA) products and daily-monthly gauge data over Bali. *International Journal of Remote Sensing*, 32(24), 8969-8982.

Brooks, S. H., 1958: A discussion of random methods for seeking maxima. *Operations Research*, 6, 244-254.

Gupta, H. V., S. Sorooshian, and P. O. Yapo, 1999: Status of automatic calibration for hydrologic models: Comparison with multilevel expert calibration. *Journal of Hydrologic Engineering*, 4(2), 135-143.

Haddeland, I., D. B. Clark, W. Franssen, F. Ludwig, F. Vob, N. W. Arnell, N. Bertrand, M. Best, S. Folwell, D. Gerten, S. Gomes, S. N. Gosling, S. Hagemann, N. Hanasaki, R. Harding, J. Heinke, P. Kabat, S. Koirala, T. Oki, J. Polcher, T. Stacke, P. Viterbo, G. P. Weedon, and P. Yeh, 2011: Multimodel estimate of the global terrestrial water balance: Setup and first results. *Journal of Hydrometeorology*, DOI:10.1175/2011JHM1324.1.

Hagemann, S. and L. Dümenill, 1998: A parameterization of the lateral waterflow for the global scale. *Climate Dynamics*, 14, 17-31.

Hagemann, S. and L. Dümenill, 2001: Validation of the hydrological cycle of ECMWF and NCEP reanalyses using the MPI hydrological discharge model. *Journal of Geophysical Research*, 106, 1503-1510.

Hong, J. B., B. S. Kim, and S. Y. Yoon, 2006: Evaluation of accuracy of the physics based distributed hydrologic model using *vflo*^{TM} Model. *KSCE Journal of Civil Engineering,* 26(6B), 573-711.

Hong, Y., K. Hsu, S. Sorooshian, and X. Gao, 2004: Precipitation estimation from remotely sensed imagery using an artificial neural network cloud classification system, *Journal of Applied Meteorology*, 43, 1834-1853.

Huffman, G. J., R. F. Adler, D. T. Bolvin, G. Gu, E. J. Nelkin, K. P. Bowman, Y. Hong, E. F. Stocker, and D. B. Wolff, 2007: The TRMM multisatellite precipitation analysis (TMPA): Quasi-global, multiyear, combined-sensor precipitation estimates at fine scales, *Journal of Hydrometeorology*, 8, 38-55.

Joyce, R., J. Janowiak, P. Arkin, and P. Xie, 2004: CMORPH: A method that produces global precipitation estimates from passive microwave and infrared data at high spatial and temporal resolution, *Journal of Hydrometeorology*, 5, 487-503.

Khan, S. I., P. Adhikari, Y. Hong, H. Vergara, T. Grout, R. F. Adler, F. Policelli, D. Irwin, T. Korme, and L. Okello, 2010: Observed and simulated hydroclimatology using distributed hydrologic model from in-situ and multi-satellite remote sensing datasets in Lake Victoria region in East Africa. *Hydrology and Earth System Sciences Discussions*, 7, 4785-4816.

Liang, X., D. P. Lettenmaier, E. F. Wood, and S. J. Burges, 1994: A simple hydrologically based model of land surface water and energy fluxes for general circulation models. *Journal of Geophysical Research*, 99(D7), 14415-14428.

Liang, X. E. F. Wood, and D. P. Lettenmaier, 1996: Surface soil moisture parameterization of the VIC-2L model: Evaluation and modification. *Global and Planetary Change*, 13, 195-206.

Moretti, G. and A. Montanari, 2007: AFFDEF: A spatially distributed grid based rainfall-runoff model for continuous time simulation of river discharge. *Environmental Modelling and Software*, 22, 823-836.

Moriasi, D. N., J. G. Arnold, M. W. Van Liew, R. L. Bingner, R. D. Harmel, and T. L. Veith, 2007: Model evaluation guidelines for systematic quantification of accuracy in watershed simulations. *Transaction of the ASABE*, 50(3), 885-900.

Nash, J. and J. Sutcliffe, 1970: River flow forecasting through conceptual models. Part I: A discussion of principles. *Journal of Hydrology*, 10, 282-290.

Park, J. H., Y. T. Hur, K. S. Ryoo, and G. S. Lee, 2010: Flood runoff simulation using GIS-grid based K-DRUM for Yongdam-Dam Watershed. KSCE *Journal of Civil Engineering*, 29(1D), 145-151.

Qin, C., Y. Jia, Z. Su, Z. Zhou, Y. Qiu, and S. Suhui, 2008: Integrating remote sensing information into a distributed hydrological model for improving water budget prediction in large-scale basins through data assimilation. Sensors, 8, 4441-4465.

Singh, J., H. V. Knapp, G. Arnold, and M. Demissie, 2005: Hydrologic modeling of the Iroquois River watershed using HSPF and SWAT. *Journal of American Water Resources Association*, 41(2), 361-375.

Sorooshian, S., R. Lawford, P. Try, W. Rossow, J. Roads, J. Polcher, G. Sommeria, and R. Schiffer, 2000: Evaluation of PERSIANN system satellite-based estimates of tropical rainfall. *Bulletin of the American Meteorological Society*, 81, 2035-2046.

Su, F., Y. Hong, and D. P. Lettenmaier, 2008: Evaluation of TRMM Multisatellite Precipitation Analysis (TMPA) and its utility in hydrologic prediction in the La Plata basin. *Journal of Hydrometeorology*, 9, 622-640.

Wang, J., Y. Hong, L. Li, J. J. Gourley, S. I. Khan, K. K. Yilmaz, R. F. Adler, F. S. Policelli, S. Habib, D. Irwin, A. S. Limaye, T. Korme, and L. Okello, 2011: The coupled routing and excess storage (CREST) distributed hydrological model. *Hydrological Sciences Journal*, 56(1), 84-98.

Zhao, R. J., 1992: The Xinanjiang model applied in China. *Journal of Hydrology*, 135(3), 371-381.

APCC TECHNICAL REPORT 2012-02

- Evaluation of Water Balance on a Regional Scale
- Analysis of Climatic Trends over South Asia
- Study of Aerosol Effect on Accelerated Snow Melting
- Aerosol Variability on Global and Regional Scales
- Evaluation of a Distributed Hydrologic Model

APEC Climate Center

12, Centum 7-ro, Haeundae-gu, Busan 612-020,
Republic of Korea
Tel: +82-51-745-3900 Fax: +82-51-745-3949
www.apcc21.org

비매품
9 788997 333370
ISBN 978-89-97333-37-0
ISBN 978-89-97333-35-6 (세트)